Journal of Civil Engineering and Urban Planning (2025)
Clausius Scientific Press, Canada

DOI: 10.23977/jceup.2025.070114
ISSN 2616-3969 Vol. 7 Num. 1

Reliability Evaluation of CRTS II Ballstless Slab Track on Bridge Considering Multiple Important Failure Modes

Li Lanxin[1], Zhang Xuanyi[1,2]

[1]*Faculty of Architecture, Civil and Transportation Engineering, Beijing University of Technology, Beijing, 100124, China*
[2]*Key Laboratory of Urban Security and Disaster Engineering of Ministry of Education, Beijing University of Technology, Beijing, 100124, China*

Keywords: CRTS II ballastless slab track; Service limit service; Time-dependent system reliability; Sensitivity analysis; Reliability evaluation

Abstract: This study systematically investigates the service reliability of the CRTS II (China Railway Track System) ballastless slab track on bridges under the serviceability limit state. The failure modes of each structural layer are comprehensively identified, and corresponding time-dependent limit state functions are established. Based on the logical relationships among these failure modes, a time-dependent system limit state function considering multiple failure mechanisms is formulated. The reliability of the track structure over its service life is analyzed, along with a sensitivity analysis of key parameters under load effects. The results demonstrate that static wheel weight and fastener resistance have significant impacts on the overall reliability of the track structure. Additionally, the degradation coefficient and correction coefficient of the CRTS II slab track play a crucial role in its reliability. These findings provide a theoretical basis and quantitative support for the reliability assessment of CRTS II ballastless slab tracks and offer valuable guidance for track maintenance and repair strategies.

1. Introduction

In China's high-speed railway systems, the CRTS II ballastless slab track has been widely adopted [1]. Thus, ensuring the service reliability of this track system throughout its entire lifecycle is of critical importance. Field investigations indicate that under the combined effects of temperature variations and train loads, although safety failure modes are relatively rare, damage such as cracking and separation gaps has been observed [2]. As these damages gradually become apparent, the normal service limit states reliability of the CRTS II slab ballastless track faces significant challenges. Such deterioration not only compromises ride comfort for high-speed trains but may also jeopardize operational safety. Therefore, it is imperative to conduct a lifecycle reliability assessment of the CRTS II slab ballastless track structure under normal service limit states.

Extensive research has been conducted by scholars on the service performance of CRTS II ballastless slab track. For instance, Cheng [3] employed nonlinear finite element analysis to evaluate the mechanical behavior of CRTS II track slabs; Chen [4] established a finite element model of CRTS II track slabs using ABAQUS software to investigate the formation mechanism of mortar gap defects

and their influence on track stress and deformation; Yan [5] conducted detailed simulation modeling studies on the mechanical characteristics of the foundation plate; Liu [6] et al., based on horizontal push plate scale-down and full-scale tests, obtained the constitutive relationship between tangential force and displacement at the interlayer interface of CRTS II ballastless slab track; Li [7] et al. analyzed the influence mechanism of interlayer shear failure through three-dimensional modeling. Additionally, other scholars have also conducted relevant research from various perspectives. These studies provide important theoretical support and practical foundations for further in-depth analysis and optimal design of track.

In actual service, the CRTS II ballastless slab track is subjected to the combined effects of train loads, temperature variations, and material properties. Zhang [8] et al. considered the effects of lateral train loads and temperature gradients, proposing a crack resistance reliability analysis method based on higher-order moments; Tong [9] et al. established a functional equation for track slab crack width under the combined action of temperature and train loads, analyzing crack width reliability using the moment method; Li [10] et al. established a limit state equation incorporating both temperature and train loads, investigating the transverse crack resistance reliability of track slabs. Zhang [11] et al. analyzed the reliability of the track slab system using higher-order moment methods. In terms of time-dependent reliability research, Zou [12,13] et al. established a time-dependent model for the transverse bending capacity of track slabs based on the third-moment method and developed a transverse crack resistance analysis approach considering single and multiple failure modes; Wang [14] et al. studied the time-dependent reliability of crack width in CRTS II foundation plate on bridges under varying temperature conditions; Tong [15] conducted time-dependent reliability studies on track slab fatigue, establishing a time-dependent reliability assessment framework considering residual stress redistribution; Zhang [16] et al. performed systematic time-dependent reliability analyses of track slabs under multiple failure modes. Despite significant progress in existing studies, current research still exhibits certain limitations, particularly in the investigation of the overall time-dependent reliability of track structures. Most studies have focused on time-dependent reliability analysis of individual structural layers rather than the integrated system behavior.

Based on this, this paper focuses on the life-cycle service reliability assessment of the CRTS II ballastless slab track structures under normal service limit states. The specific research content includes: First, identifying common failure modes of each structural layer in CRTS II ballastless slab tracks under normal service limit states. Second, constructing an overall limit state function for the track structure that accounts for multiple failure modes. Then, identifying key stochastic parameters and conducting a life-cycle service reliability assessment of the track structure based on these parameters. Finally, performing a sensitivity analysis of load effect parameters to investigate the influence of different loads on the reliability of the track structure and its individual layers. The research findings will provide a theoretical foundation and practical support for accurately assessing the service reliability and guiding the maintenance of ballastless track structures in China's high-speed railways.

2. Overall limit state functions of CRTS II ballastless slab track

Under normal service limit conditions, all structural layers of the CRTS II ballastless slab track on bridges may experience failure, primarily manifested as cracks and debonding failure modes. In this section, the common failure modes of each structural layer will first be identified, and the corresponding limit state functions will be established. Subsequently, based on multiple failure modes, an integrated limit state function for the track structure will be constructed to more comprehensively evaluate its reliability performance under normal service conditions.

2.1 Crack initiation and overwidth cracks in track slabs

The CRTS II track slab is a longitudinal continuous structural layer. Under the normal service limit state, longitudinal cracking is only allowed at the false joint [17]. Therefore, the applicability failure modes of the track slab structural layer include two types: transverse cracking and excessive longitudinal cracks. The limit state for transverse cracking is defined as the transverse bending moment M_{ts}, $h(t)$ acting on the track slab reaching the cracking limit moment $M_{cr}(t)$, where t is the time variable. Considering material performance degradation, $M_{cr}(t)$ can be simplified as the product of the initial ultimate cracking bending moment M_{cr0} and the attenuation function, resulting in the following ultimate state function [13] :

$$G_1(\mathbf{X},\mathbf{Y}(t),t)=M_{cr0}(1-k_{ts}t)-M_{ts,h}(t) \tag{1}$$

Where $\mathbf{X}$ represents the random variable; $\mathbf{Y}(t)$ represents the vector of stochastic processes ;and k_{ts} is the attenuation coefficient of the ultimate cracking bending moment. the degradation coefficient of the cracking limit moment. During service, the track slab is subjected to train loads, temperature effects, and bridge deformation effects. The transverse bending moment $M_{ts,h}$(t) induced by train loads and temperature effects can be calculated as follows [13] :

$$M_{ts,h}(t)=M_{Plt}(t)+0.3Q(t)h_a+\frac{a_{tc}E_{ct}T_g(t)h_{ts}^4}{12(1-v)} \tag{2}$$

Where $M_{plt}(t)$ represents the lateral bending moment induced by vertical train loads; $Q(t)$=0.8$P_j(t)$ denotes the lateral train load; $P_j(t)$ is the static wheel load; h_a=h_{ts}—h_c indicates the effective height of the track slab; with h_{ts}=0.3m being the thickness of the track slab and h_c=0.05m i representing the concrete cover thickness; a_{tc}=10^{-5}/℃ is the coefficient of linear thermal expansion for concrete; E_{ct}=35.5GPa stands for the elastic modulus of track slab concrete; $T_g(t)$ refers to the temperature gradient; and v=0.2 indicates the Poisson's ratio of the track slab. Due to the complexity of interlayer interactions in the track, analytical calculation of vertical train loads proves challenging. Therefore, this study employs the finite element model illustrated in Figure 1 to compute the effects of longitudinal train loads (for details, refer to [16]). Considering dynamic amplification effects, the vertical train load is taken as $\alpha_P P_j(t)$, where α_p is the dynamic correction factor for train loads.

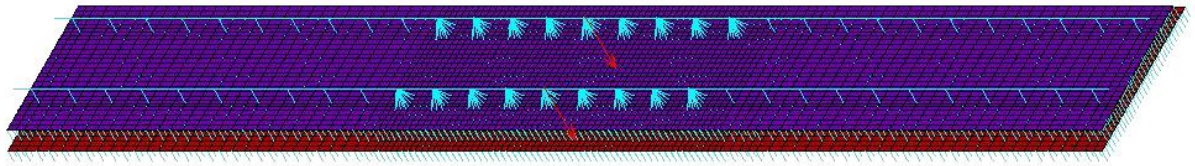

Figure 1 FE model of CRTS II ballastless slab track

According to the specification, under normal limit states, the crack width verification requirement for concrete members stipulates that the longitudinal crack width of the track slab must not exceed the permissible crack width limit [17]. Therefore, the limit state function $G_2(\mathbf{X}, \mathbf{Y}(t), t)$ for the maximum longitudinal crack width of the track slab is expressed as [12]:

$$G_2(\mathbf{X},\mathbf{Y}(t),t)=[w]-w_t(t) \tag{3}$$

Where the allowable value of crack width [w]=0.3mm is determined based on the environmental category and concrete structure requirements. Here, $w_t(t)$ represents the maximum value of the longitudinal crack width developed in the track slab under external loads, which is expressed according to the design specifications [11]:

$$w_t(t) = \alpha_{cr}\phi\frac{\sigma_s(t)}{E_s}(1.9c_s + 0.08\frac{d_{eqt}(1-\kappa_{tsl}t)}{\rho_{te}(t)}) \tag{4}$$

Where α_{cr} is the load-bearing characteristic coefficient of the member. For eccentrically tensioned reinforced concrete members, α_{cr} is taken as 2.4 according to the code; ϕ is the non-uniform strain coefficient of longitudinal tensile reinforcement between cracks, taken as 1.0 in this study; E_s is the elastic modulus of steel, taken as E_s=2.00 $\times 10^5$ N/mm²; c_s is the distance from the outer edge of the longitudinal tensile reinforcement to the bottom of the tension zone, taken as c_s=50mm based on the actual structure of the track slab; according to the reinforcement configuration of the CRTS II track slab, the equivalent diameter of the longitudinal reinforcement in the tension zone is approximately taken as d_{eqt}=8 mm, and the tensile reinforcement ratio $\rho_{te}(t) = A_{sl}(t) / A_t$; where $A_{sl}(t)$ is the cross-sectional area of the longitudinal reinforcement, calculated as $A_{sl}(t) = 6\pi[d_{eqt}(1- \kappa_{tsl}t)]$²; $\sigma_s(t)$ represents the longitudinal stress in the concrete, primarily considering the effects of temperature gradient, uniform temperature, concrete shrinkage and creep, as well as longitudinal train loads, and is calculated as follows [16][18]:

$$\sigma_{ts}(t) = \lambda_s E_s a_{ts}\Delta T(t) + \frac{\lambda_s E_s a_{ts} T_g(t) h_{ts}}{2} + \lambda_s E_s a_{ts}\Delta T_{ck} + \frac{\alpha_{cj} n_{cj} F_{cj} A_{ts} f'_{ts}}{6\pi(A_{ts} f'_{ts} + A_{fp} f'_{fp})[d_{eqt}(1-\kappa_{tsl}t)]^2} \tag{5}$$

Where λ_s represents the decay coefficient of E_s; a_{ts}=1.2×10^{-5}/°C represents the linear thermal expansion coefficient of steel; α_{cj} is the correction parameter for F_{cj}; n_{cj}=20 indicates the number of fasteners on each track slab; F_{cj} refers to the resistance force of the fasteners; f_{ts}=1.96MPa, and f_{fp}=1.43MPa are the tensile strengths of the track slab and the foundation plate, respectively; A_{fp}=0.59m^2 is the cross-sectional area of the foundation plate; $\Delta T(t)$, $T_g(t)$ and ΔT_{ck} a epresent the overall temperature difference of the track slab, the temperature gradient, and the equivalent temperature drop due to concrete shrinkage and creep.

2.2 Debonding between CRTS II track slab and CA mortar layer

The formation of debonding between the track slab and the CA mortar layer has become a relatively common phenomenon during the service life of CRTS II ballastless slab track. Since the interface between the CA mortar layer and the track slab is a bonded surface formed through sequential pouring, it tends to be a weak point in the track structure. The primary cause of gap formation is the excessive warping stress exerted on the CA mortar layer. When the actual ultimate warping stress $\sigma_q(t)$ acting on the CA mortar layer exceeds its initial ultimate warping stress σ_{q0}, a debonding is generated. Therefore, under the serviceability limit state (considering thermal effects), the limit state function for gap-induced failure between the CA mortar and the track slab can be expressed as [18]:

$$G_3(\mathbf{X}, \mathbf{Y}(t), t) = \sigma_{q0}(1-\kappa_{ca}t) - \sigma_q(t), \tag{6}$$

In the equation, the initial ultimate warping stress of CA mortar is taken as σ_{q0}=4MPa, where κ_{ca} represents the degradation coefficient of the ultimate warping stress for CA mortar. The expression for $\sigma_q(t)$ is expressed as follows:

$$\sigma_q(t) = \frac{E_{tc}\alpha_{tc}T_g(t)h_{ts}}{2(1-\nu)} \tag{7}$$

2.3 Cracking of foundation plate

Under the combined effects of temperature variations and train loads, the foundation plate in the CRTS II ballastless slab track system may develop cracks, with longitudinal cracks being the most prevalent type observed in practical engineering applications. These cracks not only accelerate the corrosion of reinforcement within the foundation plate but also reduce the effective cross-sectional area of tensile reinforcement. The corrosion of reinforcement subsequently exacerbates the cracking of the foundation plate. T Therefore, the time-dependent limit state function for longitudinal cracking of the foundation plate can be expressed as [14]:

$$G_4(\mathbf{X},\mathbf{Y}(t),t)=[w]-w_{\max}(t) \tag{8}$$

Where $w_{\max}(t)$ is the width of the longitudinal crack in the foundation plate considering the influence of steel corrosion and long-term load. According to the specification [17], the crack width shall be calculated as follows:

$$w_{\max}(t)=\alpha_{cr}\frac{\sigma_{fp}(t)}{E_s}(1.9c_{sf}+0.08\frac{\sqrt{4A_{sf}(t)/\pi}}{\rho_{tef}(t)}) \tag{9}$$

Where $\sigma_{fp}(t)$ denotes the tensile stress in longitudinal reinforcement; c_{sf} represents the concrete cover thickness at the bottom of the foundation plate, taken as c_{sf}=0.04m in this case; A_{sf} indicates the cross-sectional area of longitudinal reinforcement in the foundation plate. Under the influence of train loads, temperature gradients, and bridge deformations, the tensile stress $\sigma_{fp}(t)$ in longitudinal reinforcement shall be calculated as follows [14]:

$$\sigma_{fp}(t)=\frac{M_{plf}(t)+E_{cf}I_{fp}y_n(t)+M_{Tgf}(t)}{0.87A_{sf}(t)(H_{fp}-c_{sf})}+0.3Q(t)h_a, \tag{10}$$

Where M_{plf}(t), M_n(t)=E_{cf} I_{fp} y_n(t), and $M_{Tgf}(t)$ represent the bending moments caused by train loads, bridge deformation, and temperature gradients, respectively. $M_{plf}(t)$ is computed through finite element modeling. The steel stress at the foundation slab crack location caused by uniform temperature difference is given by $\sigma_{\Delta Tf}(t)$=$0.3Q(t)h_a$. E_{cf} is the elastic modulus of the concrete foundation plate, which is taken as E_{cf}=30GPa according to standard requirements; I_{fp} is the moment of inertia of the foundation plate, with I=5.71×10^{-4}m^4; $y_n(t)$ is the curvature of the bridge. Since the curvature of the bridge increases over time, this paper approximates it as $y_n(t)$=1/3y_0(1+0.0005t), where y_0 is the initial value of the bridge curvature at t=0.

2.4 Limit states of track structure considering multiple failure modes

Due to the failure of each structural layer in the CRTS II slab track affecting the overall structure, the track system is considered as a series system [18]. Based on the principle of equivalent extremal events [14], the limit state function of the series system can be defined as the minimum value of all critical failure modes. As shown in Eqs (1)-(10), the limit state functions of different failure modes have different dimensions, making it impossible to directly compare them to determine the minimum value. Therefore, this study adopts a dimensionless overall limit state function model [16], defining the overall limit state function of the CRTS II slab track structure on bridges as:

$$G_{track}(\mathbf{X},\mathbf{Y}(t),t)=\min[G_{ts}(\mathbf{X},\mathbf{Y}(t),t),G_d(\mathbf{X},\mathbf{Y}(t),t),G_{fp}(\mathbf{X},\mathbf{Y}(t),t)] \tag{11}$$

Where $G_{ts}(\mathbf{X},\mathbf{Y}(t),t)$, $G_d(\mathbf{X},\mathbf{Y}(t),t)$ and $G_{fp}(\mathbf{X},\mathbf{Y}(t),t)$ represent the equivalent dimensionless limit state functions related to the failure of the track slab, the debonding between the track slab and

CA mortar layer, and the cracking of the foundation plate:

$$G_{ts}(\mathbf{X},\mathbf{Y}(t),t)=\min[G_1(\mathbf{X},\mathbf{Y}(t),t),G_2(\mathbf{X},\mathbf{Y}(t),t)] \tag{12}$$

$$G_d(\mathbf{X},\mathbf{Y}(t),t)=1-\frac{\sigma_q(t)}{\sigma_{uq}(1-\kappa_{ca}t)} \tag{13}$$

$$G_{fp}(\mathbf{X},\mathbf{Y}(t),t)=1-\frac{w_{lp}(t)}{[w]} \tag{14}$$

3. MPHI2-GLO time- dependent reliability analysis method

Define the event of crossing from the safe domain through the limit state to the failure domain as G(**X**, **Y**(*t*), *t*). Thus, the failure event E_f within the time interval [0, *T*] can be expressed as either failure at the initial moment or the occurrence of at least one excursion event during (0, *T*]. T Accordingly, the cumulative failure probability $P_{f,c}(0, T)$ over the interval [0, *T*] is defined as:

$$P_{f,c}(0,T)=\text{Prob}[\{G(\mathbf{X},\mathbf{Y}(0),0)\le 0\}\cup\{N^+(0,T)>0\}] \tag{15}$$

Where $N^+(0,T)$ denotes the number of excursions within the interval (0,*T*], and Prob[-] represents the probability of occurrence for the event enclosed in the brackets. Regarding Eq.(15) classical theoretical analysis provides an upper bound for $P_{f,c}(0,T)$ as:

$$P_{f,c}(0,T)\le P_{f,i}(0)+\int_0^T v^+(t)dt \tag{16}$$

Where $P_{f,c}(0,T)=P_{rob}$[G(**X**, **Y**(0),0) ≤ 0] represents the instantaneous failure probability at *t*=0, which is calculated using the higher-order moment method. $v^+(t)$ denotes the excursion rate at time *t*. Since the time-domain integral of $v^+(t)$ generally lacks an analytical solution, Zhang et al. [16] introduced the Gaussian Laguerre quadrature method to express $P_{f,c}(0,T)$ as:

$$P_{f,c}(0,T)\le P_{f,i}(0)+\frac{T}{2}\sum_{k=1}^{n}v^+(t_k)\omega_k \tag{17}$$

Where *n* denotes the number of estimation points in the Gaussian-Legendre integration method, $t_k=T\cdot\tau_k/2+T/2$ represents the selected instantaneous time point, τ_k and ω_k are the *k-th* abscissa and its corresponding weight, respectively. Generally, setting *n* between 3 and 5 ensures the accuracy of the Gaussian-Legendre integration method. To balance computational efficiency and precision, this study adopts *n*=4 and abscissas $\tau_k=\{0, \pm 0.7756\}$and with weights $\omega_k=\{0.8889,0.5556\}$.

Since the calculation in this study involves relatively complex finite element analysis, the MPHI2 method is adopted to calculate $v^+(t)$ which can separate finite element analysis from time-dependent reliability assessment. The expression is [19]:

$$v^+(\tau)=\frac{\Phi_2[\beta_M(\tau),-\beta_M(\tau+\Delta\tau);\rho_{GM}(\tau,\tau+\Delta\tau)]}{\Delta\tau} \tag{18}$$

Where $\Phi_2(\ ;\ ;\ )$ represents the two-dimensional cumulative normal distribution function; $\Delta\tau$ is the time increment, selected such that the autocorrelation coefficients of each component of **Y**(*t*) fall within the range [0.99,0.995]; $\beta_M(t)$ and $\beta_M(t+\Delta t)$ are reliability indicators calculated based on the first four moments of $G_{01}(\mathbf{X},\mathbf{Y}(\tau),\tau)$ and $G_{02}(\mathbf{X},\mathbf{Y}(\tau+\Delta\tau),\tau+\Delta\tau)$; $G_{01}(\mathbf{X},\mathbf{Y}(\tau),\tau)$ and $G_{02}(\mathbf{X},\mathbf{Y}(\tau+\Delta\tau),\tau+\Delta\tau)$ are time-invariant limit state functions at fixed times τ and $\tau+\Delta\tau$ obtained by treating the time *t* in all limit state functions as a constant, abbreviated as G_{01} and G_{02}; the correlation coefficient between G_{01} and-G_{02} in Gaussian space is expressed as:

$$\rho_{GM}(\tau,\tau+\Delta\tau)=\mathrm{FMTC}[\rho_{G0}(\tau,\tau+\Delta\tau)],\ \rho_{G0}(\tau,\tau+\Delta\tau)=\frac{\mu_{G_{01}}\mu_{G_{02}}-E[G_{01}G_{02}]}{\sigma_{G_{01}}\sigma_{G_{02}}} \tag{19}$$

Where $\rho_{G0}(\tau,\tau+\Delta\tau)$ denotes the autocorrelation coefficient between G_{01} and-G_{02} in the general space $\rho_{G0}(\tau,\tau+\Delta\tau)$ in general space; FMTC[·] represents the normal transformation based on the first four moments of G_{01} and-G_{02}; $\mu_{G_{01}},\mu_{G_{02}}$ and $\sigma_{G_{02}},\sigma_{G_{01}}$ are the mean values and standard deviations of G_{01} and G_{02}, respectively, which can be computed using the point estimation method combined with the bivariate dimension reduction method (BDRM) [16].

4. Time-dependent reliability analysis of CRTS II ballastless slab track system

4.1 Statistical information of random parameters

An analysis of Eqs. (11)-(14) reveals that the global limit state function of CRTS II ballastless slab track involves multiple parameters and requires finite element analysis. To improve computational efficiency, this study treats load-related parameters as random variables while considering material parameters as deterministic values.

The load effects considered in this study include temperature, train loads, and bridge deformations. Notably, the temperature effect exhibits time-dependent characteristics and is modeled as a stochastic process. The statistical data are categorized into four seasonal groups, as presented in Table 2. The autocorrelation functions for temperature gradient and uniform temperature are expressed as follows:

$$\rho_{T_g}(\Delta t)=\exp(-\Delta t^2/l_t^2) \tag{20}$$

$$\rho_{\Delta T}(\Delta t)=\exp(-0.1|\Delta t|/l_t) \tag{21}$$

$\rho_{T_g}(\Delta t)$ and $\rho_{\Delta T}(\Delta t)$ represent the autocorrelation functions of $T_g(t)$ and $\Delta T(t)$ in Gaussian space; l_t =6 months denotes the correlation length of the temperature load. Since both $T_g(t)$ and $\Delta T(t)$ share environmental temperature as their common source of randomness, they exhibit significant correlation. The correlation function is assumed as [16]:

$$\rho_{\Delta TT_g}(\Delta t)=\alpha_{\Delta TT_g}\exp(-0.1\Delta t^2/l_t^2) \tag{22}$$

Where $\rho_{\Delta TT_g}(\Delta t)$ is the correlation coefficient between $\Delta T(t)$ and $T_g(t)$ in Gaussian space; $\alpha_{\Delta TT_g}$ is $\rho_{\Delta TT_g}(\Delta t)$ parameter, and its values in different quarters are shown in Table 1 [19].

Table 1 Statistical information of temperature load

Month	T_g (t) (℃ /m)					ΔT(t) (℃)				
	Distribution	Mean	COV	ACF	$\alpha_{\Delta TT_g}$	Distribution	Mean	COV	ACF	$\alpha_{\Delta TT_g}$
Jan.-Mar.	Weibull	33.96	0.14	Eq. (20)	0.1495	Normal	−23.19	0.08	Eq. (21)	0.1495
Apr.-Jun.		−18.40	0.23		0.6677		7.27	0.18		0.6677
Jul.-Sep.		40.68	0.16		0.6668		7.27	0.18		0.6668
Oct.-Dec.		−19.43	0.31		0.1528		−23.19	0.08		0.1528

The Static wheel weight $P_j(t)$ reflects the uncertainty of train loads in both lateral and longitudinal directions, while the uncertainty of train braking force is represented by the fastener resistance F_{cj}. Additionally, the initial curvature y_0 of the bridge also has uncertainty and is therefore considered a random variable. In summary, the key parameters characterizing the random uncertainty of load effects include P_j, F_{cj}, ΔT_{ck}, and y_0, with their statistical information detailed in Table 2. The autocorrelation function of $P_j(t)$ can be approximately expressed as:

$$\rho_{P_j}(\Delta t) = \exp(-\Delta t^2 / l_{P_j}^2) \tag{23}$$

Where $l_{P_j} = 4$ month is the relevant length of $P_j(t)$.

Table 2 Statistical information of random variables

Parameters	Distribution	Mean	COV	ACF
P_j(t) (kN)	Normal	119	0.2	Eq. (23)
F_{cj} (kN/m)	Lognormal	12	0.3	-
ΔT_{ck} (℃)	Lognormal	10	0.1	-
y_0 (m^{-1})	Lognormal	0.002	0.25	-

4.2 Overall time-dependent reliability analysis

Through the overall limit state function Eq. (11) e established in Eq. (11), the MPHI2-GLO method was employed to calculate the failure probability of CRTS II ballastless slab track under normal service limit conditions. The cumulative failure probabilities $P_{f,c}$(0,T) at different service years was obtained, with its variation trend shown in Fig. 2. To compare the failure probabilities of each structural layer with the overall failure probability of the track structure, the cumulative failure probabilities of each structural layer are also plotted in Figure 2. The following observations can be made from Fig. 2:

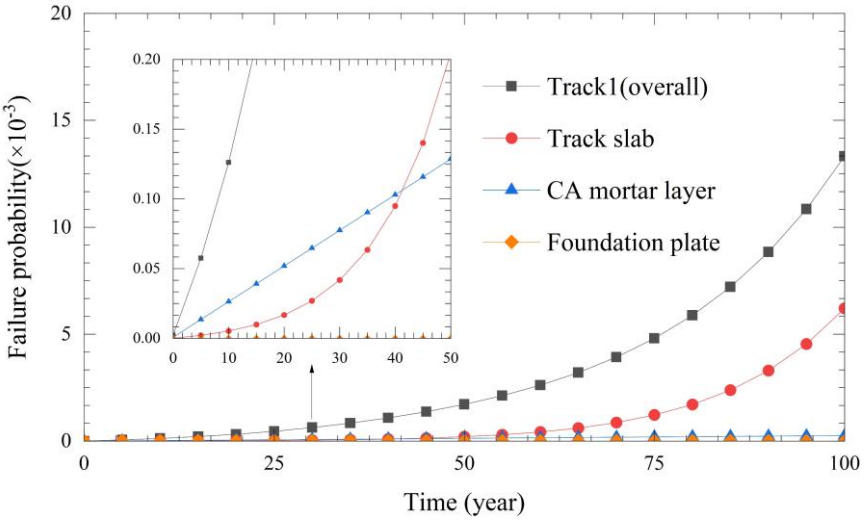

Figure 2 Failure probability of CRTS II ballastless track system and comparative analysis under normal service limit state

(1) Under normal service conditions, the cumulative failure probability of the CRTS II ballastless slab track structure is positively correlated with the service life. Analysis results show that, without maintenance and repair, the cumulative failure probabilities over 60 and 100 years of service are 0.0026 and 0.0133, respectively, indicating relatively high failure probabilities. This suggests that enhanced maintenance and repair are crucial for controlling the failure probability.

(2) The failure probability of different structural layers varies with the service life. In the first 40 years of service, the failure probability of the CA mortar layer is higher compared to other structural layers, while the failure probabilities of the track slab and foundation plate are lower; after 40 years of service, the failure probability of the track slab exceeds that of the CA mortar layer, becoming the most prone to failure among all structural layers. This change is closely related to the degradation patterns of materials in each structural layer.

(3) The overall failure probability of the CRTS II ballastless slab track structure is greater than

that of each individual structural layer. After 60 years of service, the overall failure probability of the track structure is 0.0026, while the failure probabilities for the track slab and CA mortar layer are 0.0004 and 0.0001, respectively. The overall failure probability is approximately 6.5 times and 26 times that of the track slab and CA mortar layer, respectively; after 100 years of service, the overall failure probability of the track structure is 0.0133, with the failure probabilities for the track slab and CA mortar layer being 0.0062 and 0.0002, respectively. The overall failure probability is approximately 2.1 times and 6.7 times that of the track slab and CA mortar layer, respectively.

4.3 Parameter sensitivity analysis

To more comprehensively study the service reliability of CRTS II ballastless slab track, this section conducts sensitivity analysis on key parameters of load effects (Table 2). To ensure the reliability of the structure over its service life, this section selects two time points: 60 years and 100 years for analysis, to comprehensively evaluate the sensitivity of each parameter. By keeping the variances of each parameter constant and only adjusting their means, we explore the trends in the cumulative failure probability of the track structure as a whole over the 60-year and 100-year service periods, with different parameter mean values[20]. The relevant results are shown in Figures 3 and 4. As can be seen from the figures:

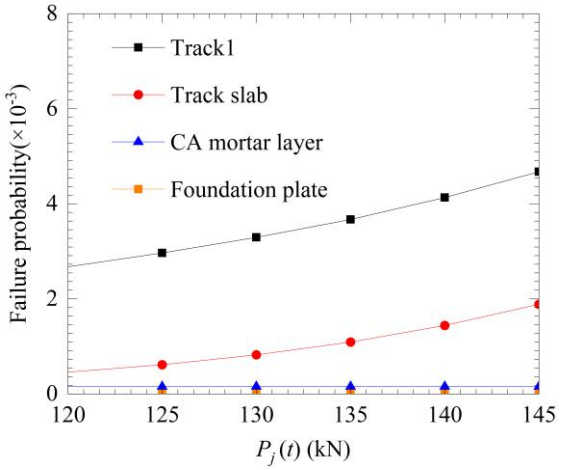

(a) Static wheel weight

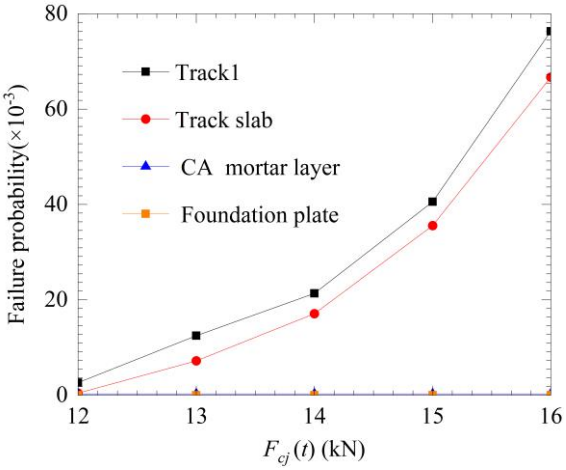

(b) Fastener resistance

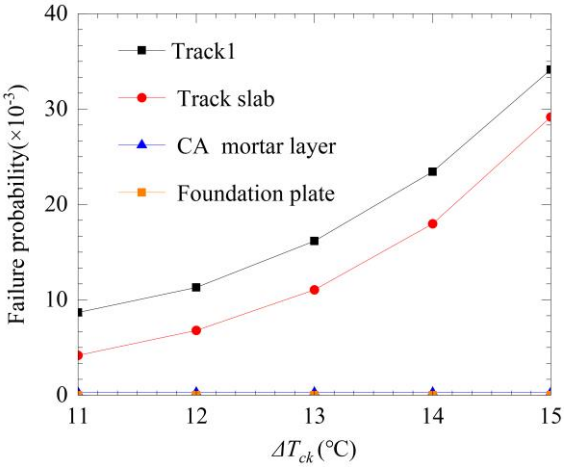

(c) Thermal equivalent method for concrete shrinkage and creep

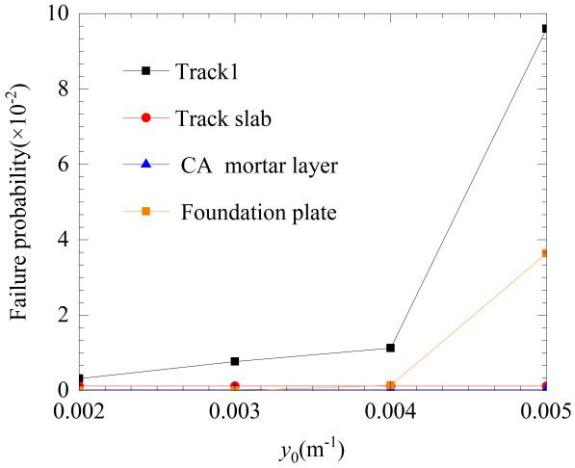

(d) Initial bridge curvature

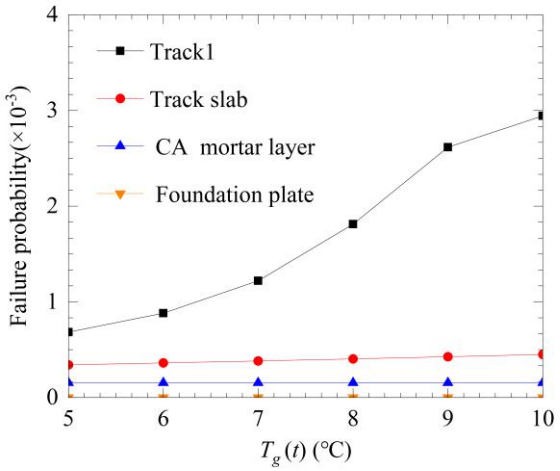

(e) Temperature gradient

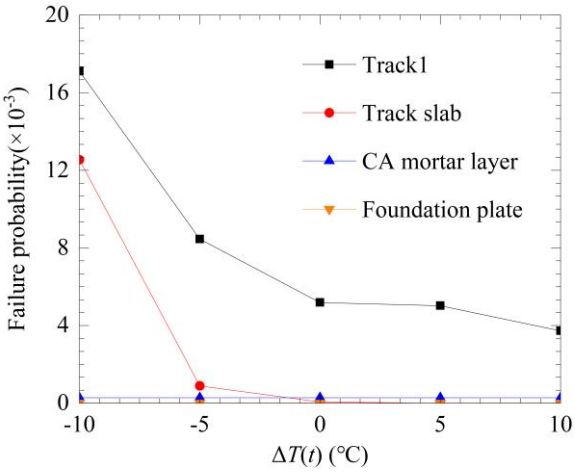

(f) Global temperature difference

Figure 3 Failure probability with each factor during 60 years of service

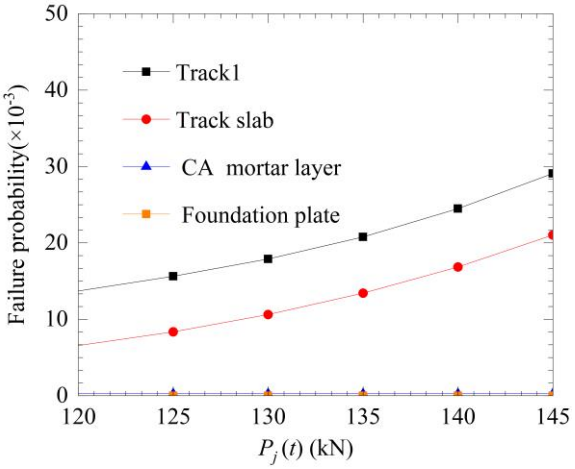

(a) Static wheel weight

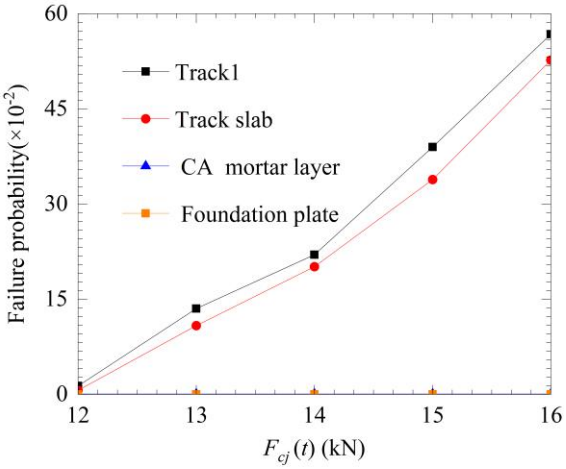

(b) Fastener resistance

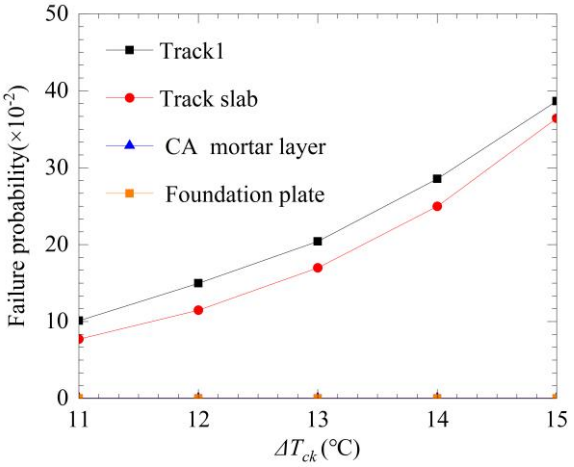

(c) Thermal equivalent method for concrete shrinkage and creep

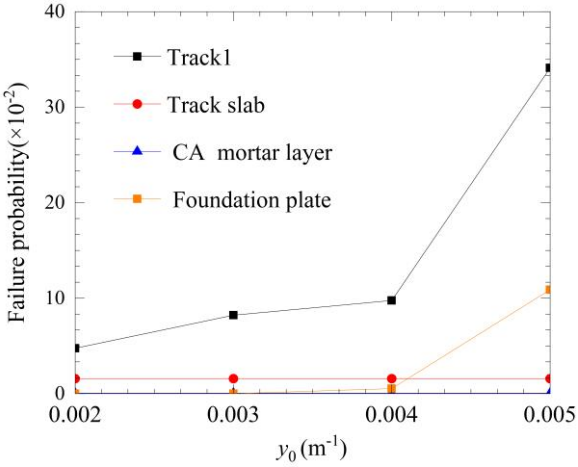

(d) Initial bridge curvature

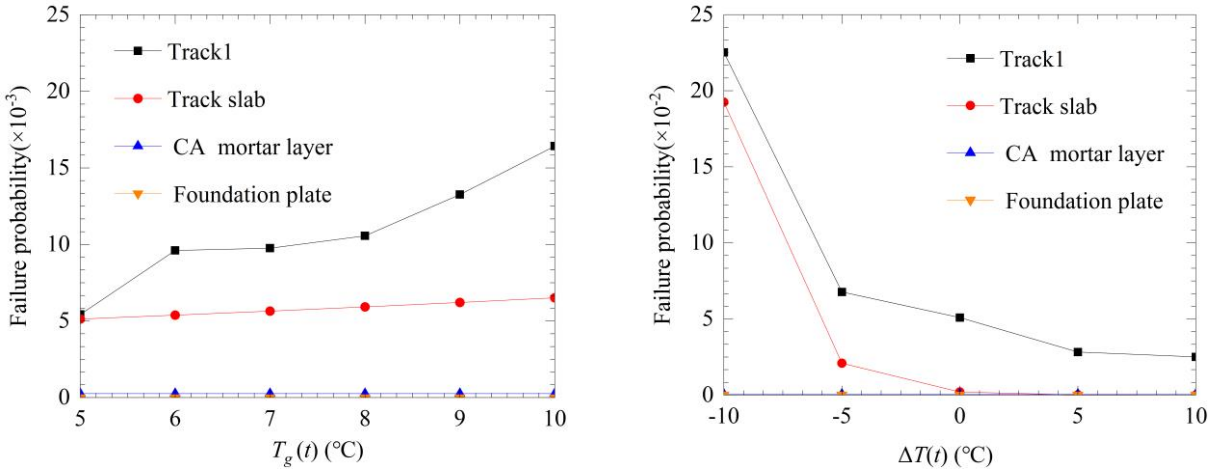

(e) Temperature gradient (f) Global temperature difference

Figure 4 Failure probability with each factor during 100 years of service

From the analysis of Figure 3 and 4 (a) to (f), it can be obtained that:

(1) With the increase of static wheel weight, the failure probability of track slab and overall track structure increases. Static wheel weight is proportional to train load, and the increase of load aggravates the occurrence of transverse cracking of track slab, thus leading to the increase of failure probability of track slab and then increasing the failure probability of overall track structure.

(2) Increasing the resistance of the fasteners will increase the failure probability of the track slab and the overall track structure. After the resistance of the fasteners increases, the longitudinal tensile stress of the track slab under the longitudinal train load increases, which is not conducive to the control of the longitudinal cracks of the track slab and further promotes the increase of the failure probability.

(3) The increase of equivalent temperature drop due to concrete shrinkage and creep will lead to the increase of longitudinal tensile stress of track slab, which will adversely affect the control of longitudinal crack width of track slab, and eventually lead to the increase of track slab failure probability, which will negatively affect the reliability of the overall track structure.

(4) As the initial curvature of the bridge increases, both the failure probability of the foundation plate and the overall track structure show an upward trend. The increase in initial curvature leads to greater tensile stress on the longitudinal reinforcement of the foundation plate, which in turn exacerbates the expansion of crack widths, increasing the failure probability and affecting the reliability of the entire track structure.

(5) The increase of temperature gradient has a negative impact on the track slab and the overall track structure. The increase of temperature gradient will cause the transverse bending moment and longitudinal tensile stress of the track slab to increase, which will further aggravate the transverse cracking of the track slab and the width of the longitudinal cracks, thus leading to the increase of the failure probability of the track slab.

(6) As the overall temperature difference increases, the failure probability of track panels and the overall track structure decreases. Negative temperature differences are more detrimental than positive ones, as the overall temperature difference affects the thermal effects caused by longitudinal train loads, which in turn adversely impacts the cracking of track panels, leading to a decrease in failure probability with increasing overall temperature difference.

(7) Over a 60-year and 100-year service period, the failure probability changes similarly with each parameter, but the magnitude of change differs. For example, when the overall temperature difference increases from-10 ℃-10 ℃, the difference in failure probability over a 60-year service period is 0.0134, while over a 100-year service period it is 0.2001, with the change magnitude being

approximately 15 times that of the 60-year period. Therefore, during long service periods, particular attention should be paid to the variation in failure probability.

(8) When comparing the effects of various parameters horizontally, the equivalent temperature drops due to static wheel weight, fastener resistance, concrete shrinkage and creep, and initial bridge curvature over a 60-year service life are 0.0062,0.0105,0.0057, and 0.0051, respectively; over a 100-year service life, these increments are 0.0726,0.1280,0.0809, and 0.0688, respectively. Therefore, fastener resistance has the greatest impact on the failure probability. Thus, in practical applications, particular attention should be paid to the magnitude of fastener resistance to ensure the long-term reliability of CRTS II ballastless slab track.

5. Conclusions

This study identifies common failure modes of CRTS II ballastless slab track structures under normal service limit conditions and establishes limit state functions for each failure mode. Based on the logical relationships between these failure modes, an overall ultimate state function for the track under multiple failure modes is constructed. The overall reliability of the track structure is analyzed using the MPHI2-GLO time-dependent reliability method, and the influence patterns of key parameters on the time-dependent reliability of the track structure under these failure modes are explored. The research results are as follows:

(1) During the service period, the overall failure probability of CRTS II ballastless slab track is significantly higher than that of each single structural layer, but the overall system can still maintain good reliability, and the failure probability is within the allowable range.

(2) As the service life changes, the failure probabilities of different structural layers under several common failure modes vary. During the period from 0-40 years, the failure probability of the CA mortar layer is relatively high; however, from 40-100 years, the failure probability of the track slab shows a more significant increase, estimated at about three times that of the period from 0-40 years. Throughout the entire service life from 0-100 years, the failure probability of the foundation plate is generally lower than that of other structural layers, demonstrating relatively excellent safety.

(3) The overall failure probability of Type CRTS II slab ballastless track shows a certain positive correlation with static wheel load, fastener resistance, equivalent temperature drop due to concrete shrinkage and creep, and initial bridge curvature; the failure probability of the track slab is proportional to the equivalent temperature drop due to concrete shrinkage and creep, while the failure probability of the foundation plate is strongly related to the initial bridge curvature. Under the same parameter variation range, fastener resistance has a significant impact on the overall failure probability of the track structure.

References

[1] Guo Gaoran, Cui Xuhao, Du Bowen. Monitoring Technology for Deformation of Key Sections of CRTS // Slab Ballastless Track Foundation [J]. China Railway, 2019 (11):60-67.

[2] Zhao Lei. Failure Analysis and Experimental Study of Damage for CRTS II Ballastless Track Structure in High Speed Railway [D]. Nanjing: Southeast University, 2017.

[3] Cheng Qian. Study on the force performance of CRTS II type ballastless track slab for high-speed railway [D]. Zhengzhou: Zhengzhou University, 2011.

[4] Chen Long. Study on Rules and Influence of Interface Connection damage of the CRTS II Ballastless Slab [D]. Shijiazhuang: Shijiazhuang Tiedao University, 2015.

[5] Yan Bin, Cheng Ruiqi, Xie Haoran, et al. Mechanical characteristics of CRTS // ballastless track on bridge due to extreme temperature load [J]. Journal of Railway Science and Engineering, 2021,18 (04):830-836.

[6] Liu Xuewen, Gu Yonglei, Liu Yu. Horizontal Push Plate Test and Simulation of CRTS // Slab Ballastless Track [J]. China Railway, 2022, (02): 7-14.

[7] Li Yang, Chen Jinjie, Wang Jianxi, et al. Study on the Shear Failure Law of CRTS // Slab Track Layers under the Action of Braking Force [J]. China Railway, 2019, (02):47-53.
[8] Zhang Longwen, Zhou Jin. Reliability on crack resistance of CRTS II track slab based on high-order moment method [J]. Journal of Sun Yat-sen university (natural science edition), 2020,59(3):134-142.
[9] Tong Mingna, Lu Zhaohui, Zhao Yangang, et al. Reliability Evaluation of Crack Width of CRTS II Ballastless Track Slab Using Method of Moment [J]. Journal of China Railway Society, 2020,42(11):130-138.
[10] Li Hualong, Zhao Pingrui, Liu Zhibin. Research on Calculation Method of Lateral Reliability of CRTS II Ballastless Track Slab [J]. Railway Construction, 2015(03): 98-102.
[11] Zhang Xianyi, Wang Jiquan, Lu Zhaohui, et al. System Reliability of CRTS // Track Slab Considering Serviceability Limit State [J]. Journal of China Railway Society, 2022,44(12):89-96.
[12] Zou Hong, Lu Chaohui, Yu Zhiwu. Time-dependent Reliability Analysis of Transverse Cracking of CRTS II Ballastless Track Slab Using Third-moment Method *[J]. Journal of China Railway Society, 2019,41(4):177-185.*
[13] Zou Hong, Lu Chaohui, Yu Zhiwu. Reliability Evaluation of Transverse Flexural Strength of CRTS II Ballastless Track Slab Using Method of Moment [J]. Journal of China Railway Society, 2018,40(10):103-110.
[14] Wang Haopeng, Zhang Xuan Yi, Zhao Yangang. Time-dependent reliability of crack width of CRTS II foundation plate on bridge [J]. China Civil Engineering Journal, 2022,55(5):7-15.
[15] Tong Mingna, Lu Zhaohui, Zhao Yangang, et al. Reliability Evaluation of Crack Width of CRTS II Ballastless Track Slab Using Method of Moment [J]. Journal of China Railway Society, 2020,42(10):92-100.
[16] Zhang Xuan-Yi, Lu Zhao-Hui, Zhao Yan-Gang, et al. Reliability analysis of CRTS II track slab considering multiple failure modes [J]. Engineering Structures,2021,228:111557.
[17] China Academy of Building Sciences. Code for Design of Concrete Structures (GB50010-2010)[S]. Beijing: China Architecture and Building Press, 2011.
[18] Zhang Xuan-Yi, Lu Zhao-Hui, Zhao Yan-Gang, et al. Conditional time-dependent limit state function model considering damages and its application in reliability evaluation of CRTS II track slab [J]. Applied Mathematical Modelling,2022,101:654-672.
[19] Yang, Wei, Hassan Baji, and Li Chun-Qing. A Theoretical Framework for Risk–Cost-Optimized Maintenance Strategy for Structures [J]. International Journal of Civil Engineering, 2020, 18: 261-278.
[20] Industry Code of the People's Republic of China. Code for Design of High Speed Railway (TB10621-2014) [S]. China Railway Publishing House, 2014.